




Application of TENIS and artificial neural networks in neutron spectroscopy for BNCT beams in IRT-T and TRR: additional research

S. Bagherzadeh-Atashchi¹, N. Ghal-Eh^{1,a} , F. Rahmani², R. Izadi-Najafabadi¹, S. V. Bedenko³, C. H. Ordoñez⁴

¹ Department of Physics, Faculty of Science, Ferdowsi University of Mashhad, P.O. Box 91775-1436, Mashhad, Iran

² Department of Physics, K. N. Toosi University of Technology, P.O. Box 16315-1618, Tehran, Iran

³ School of Nuclear Science and Engineering, Tomsk Polytechnic University, P.O. Box 634050, Tomsk, Russian Federation

⁴ Energy Engineering Department, Bilbao Engineering School, University of the Basque Country UPV/EHU, P.O. Box 48013, Bilbao, Spain

Received: 4 July 2025 / Accepted: 29 August 2025

© The Author(s), under exclusive licence to Società Italiana di Fisica and Springer-Verlag GmbH Germany, part of Springer Nature 2025

Abstract Following the successful results of the ThErmal Neutron Imaging System (TENIS) for mono- and poly-energetic neutron sources, in this research, real-time data obtained from the TENIS were utilized for neutron spectroscopy at the exits of the Beam Shaping Assemblies (BSAs) located at the beam ports of Tomsk Polytechnic University Research Reactor (IRT-T) and Tehran Research Reactor (TRR). To achieve this purpose, 70-pixel thermal neutron images were generated for 109 mono-energetic neutrons, referred to as the neutron fluence response matrix, using the MCNP6.1 code. These images were used as the input of the artificial neural network (ANN) tools in MATLAB. Results indicated that the sigmoid transfer function in both hidden and output layers gives the best correlation between the predicted and actual spectra of Boron Neutron Capture Therapy (BNCT) beam lines in IRT-T and TRR, with correlation coefficients (R^2) of 0.74 and 0.86, and root-mean-square error of 0.020 and 0.014, respectively (*i.e.*, a max–min problem). The results suggest that the ANN-unfolded TENIS results can also accurately predict the energy spectrum of neutrons suitable for the BNCT.

1 Introduction

Boron Neutron Capture Therapy (BNCT) represents a highly effective and promising modality for cancer treatment. Various neutron sources have been investigated and employed for BNCT, with nuclear reactors being considered the most efficient option due to their high neutron flux [1, 2]. Additionally, accelerator-based sources capable of producing epithermal neutrons have been developed and utilized [3–8]. While proton therapy remains a preferred treatment for certain deep-seated tumors [9], its clinical efficacy in treating complex cases such as glioblastoma multiforme and melanoma has yielded inconclusive results, thus limiting its adoption as a standard cancer treatment. Given these considerations, ongoing research into reactor-based BNCT remains vital and warrants further exploration to optimize its therapeutic potential.

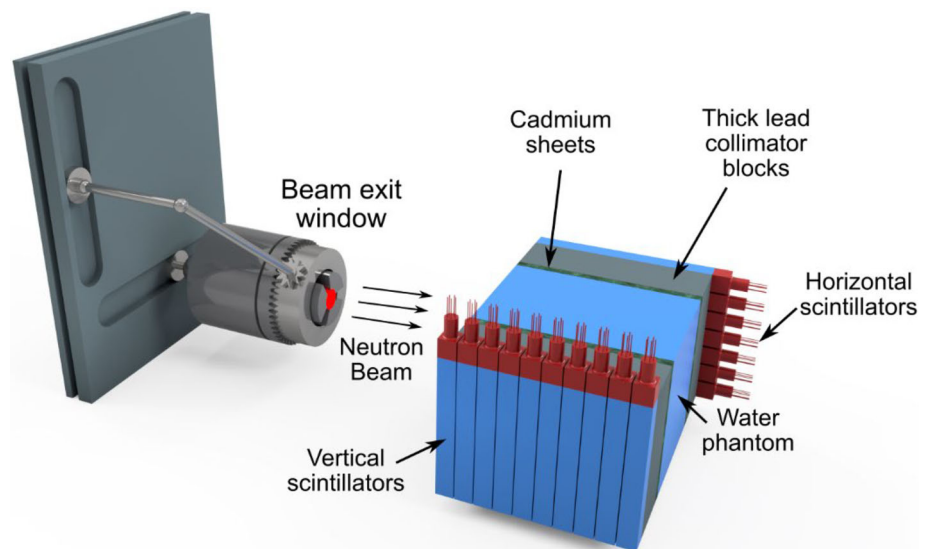
BNCT is currently under development at the IRT-T research reactor [10–12] and the Tehran Research Reactor (TRR) [13–15]. In a study by Kasesaz et al., it was demonstrated that the complete removal of graphite moderator blocks from the thermal column, followed by the installation of an appropriate Beam Shaping Assembly (BSA), enables the production of an optimized therapeutic neutron beam line. Additionally, previous work by Bagherzadeh et al. [10] involved computational modifications of the neutron beam exit window in the horizontal experimental channel (HEC-1) of the IRT-T reactor, as well as enhancements to its therapeutic beam line for BNCT applications. These studies highlight the ongoing need for advanced instrumentation capable of accurately measuring both the spectral and integral properties of neutron therapeutic beams and associated dose distributions.

It is important to emphasize that, despite extensive research and numerous clinical trials involving the IRT-T and TRR reactors, the comprehensive channel design, including the BSA, real-time imaging system, and quality control mechanisms, remains incomplete and warrants further development, which will be addressed in this study. The proposed diagnostic tools for BSA aim to enable objective, real-time assessment of treatment quality and delivered dose, enhancing the precision and safety of therapy.

Currently, a variety of commercial and specialized neutron spectrometry and dosimetry equipment for BNCT are available and suitable for this study [16–26]. Notably, spectroscopy instruments, both real-time and passive, are used for pre- and post-treatment measurements. However, most commercially available spectrometers do not meet the desired levels of accuracy and resolution necessary for precise dosimetry. Neutron spectrometers specifically designed for BNCT require rigorous scientific and technical validation, in accordance with International Atomic Energy Agency (IAEA) standards. To address these limitations, we propose

^a e-mail: ghal-eh@um.ac.ir (corresponding author)

Fig. 1 Schematic representation of beam exit window of a variable-geometry BSA (vBSA) and TENIS components [16, 27]



an innovative approach that leverages the ThERmal Neutron Imaging System (TENIS) as an intelligent diagnostic tool for quality control and real-time dosimetry (Fig. 1).

TENIS is a neutron spectrometer specifically developed to address the challenges associated with clinical BNCT, while conforming to the IAEA requirements for beam quality and dosimetric characteristics. It has demonstrated reliability in experimental campaigns using both reactor-based sources [10, 28] and radioisotope neutron sources [16, 29]. Furthermore, previous studies have shown that TENIS is a robust tool for characterizing the energy spectra of neutron beams and measuring absorbed doses [27]. Beyond BNCT, TENIS has also been utilized in thermal neutron imaging and for monitoring plasma energy losses in deuterium–tritium accelerators [30, 31].

The objective of this research is to validate the feasibility of using TENIS to support the clinical implementation of BNCT at the IRT-T and TRR research reactors. The evaluation follows a multi-step procedure: (1) A position-sensitive, rectangular array of scintillation detectors records both photon and neutron radiations at the BSAs exits. (2) TENIS then discriminates between neutron and photon signals, followed by 2D visualization of the neutron component within the therapeutic energy range. (3) The resulting neutron images are processed as input data for Artificial Neural Network (ANN)-based spectral unfolding. (4) ANN and MATLAB-based algorithms are applied to solve a max–min optimization problem, aiming to reconstruct the neutron spectra of the IRT-T and TRR beamlines. (5) Within this framework, the optimal architecture of a multilayer ANN is determined to enhance the correlation between predicted and actual BNCT spectra.

The following sections present the computational models of the IRT-T HEC-1 channel and the TRR irradiation column, including the upgraded BSA configurations and the resulting therapeutic beam parameters. Comparative analyses of the simulated beam characteristics and the experimental results, obtained via TENIS-based spectrum unfolding and ANN processing, are also discussed, along with the corresponding verification procedures.

2 Materials and methods

2.1 IRT-T epithermal beam

The IRT-T is a 6 MW_{th} pool-type research reactor that serves as an intense source of both neutrons and gamma-rays. As illustrated in Fig. 2, the reactor is designed to support a broad range of scientific and applied research activities. These include studies in solid-state physics, neutron activation analysis for elemental composition determination, radioisotope production, silicon doping, neutron radiography, and other applications involving reactor-based radiation. Its versatile configuration and high neutron flux make the IRT-T a valuable platform for both fundamental research and technological development.

The reactor core of the IRT-T is composed of IRT-3 M-type fuel assemblies, characterized by a high neutron multiplication factor and short migration length. This enables a compact core geometry with substantial neutron leakage into the reflector and the horizontal experimental channel HEC-1. Beryllium is employed as a reflector due to its long neutron migration length, which contributes to a high neutron flux density within the HEC region.

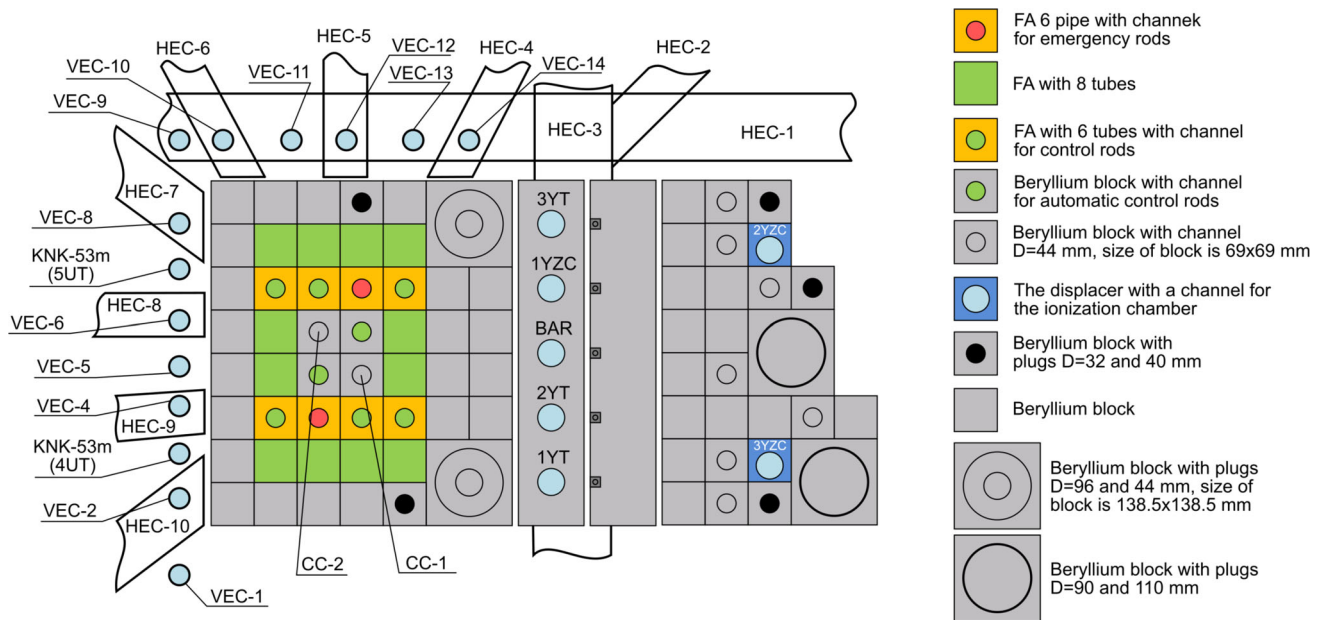


Fig. 2 Schematic layout of the IRT-T reactor core and associated experimental channels. The diagram highlights the configuration of fuel assemblies, control elements, irradiation positions, and beam ports used for neutron and gamma-ray experiments [11]

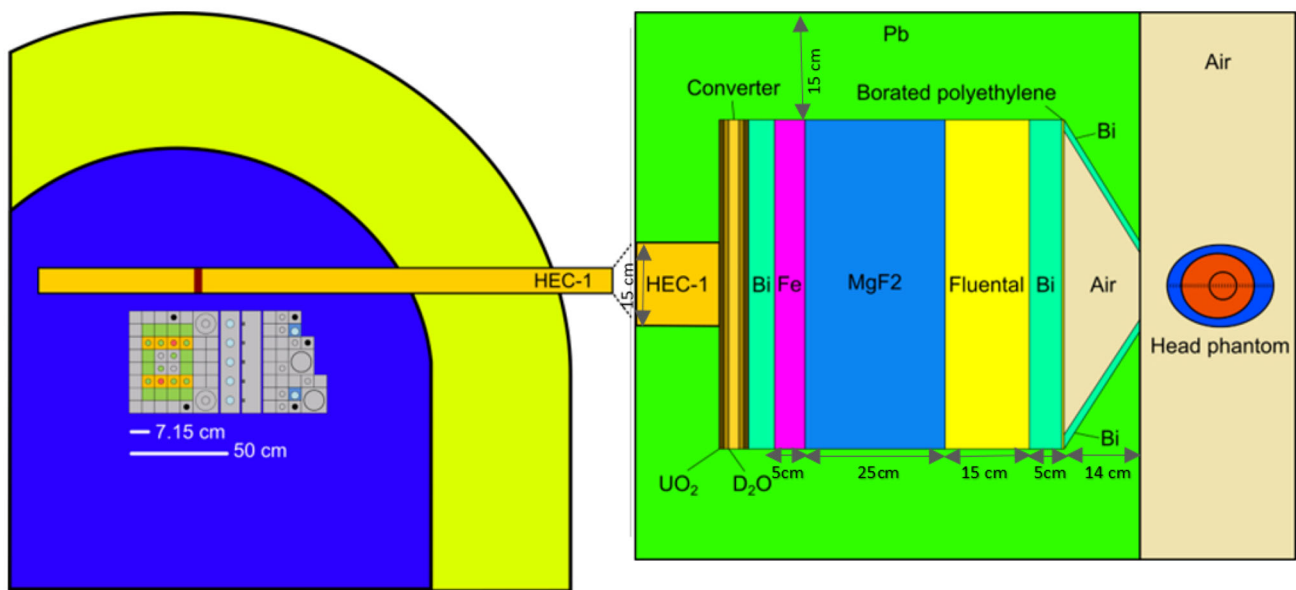


Fig. 3 Layout of the HEC-1 channel of the IRT-T reactor, showing the therapeutic beam line configuration and the proposed design of the modernized BSA. The diagram illustrates the key components involved in neutron beam extraction, collimation, and spectral tailoring for BNCT applications

Despite its compact size, the IRT-T core accommodates 14 vertical experimental channels (VECs) and 10 horizontal experimental channels (HECs), a number that exceeds those available in many higher-power research reactors. This configuration enables the simultaneous irradiation of a large number of experimental targets.

A distinguishing feature of the IRT-T reactor is its pronounced epithermal neutron component, resulting from the use of a beryllium moderator and the strategic placement of beryllium traps in the central channel region. This spectral characteristic makes the IRT-T particularly well-suited for applications such as BNCT, setting it apart from other research reactors in this field (Fig. 3). See the basic configuration in [10].

The therapeutic beam line and the proposed BSA were modeled using the MCU5TPU software package. MCU (Monte Carlo Universal) is a general-purpose Monte Carlo code designed for simulating the transport of neutrons, photons, electrons, and positrons in three-dimensional geometries [32]. The code utilizes two nuclear data libraries: (1) the primary database, MCUDB50, which

Fig. 4 Schematic of the modified thermal column at the TRR, illustrating the therapeutic beam line and the proposed BSA configuration for BNCT. The design, based on [14], includes a layered arrangement of moderator, reflector, thermal neutron filters, and gamma-ray shields to optimize epithermal neutron beam production

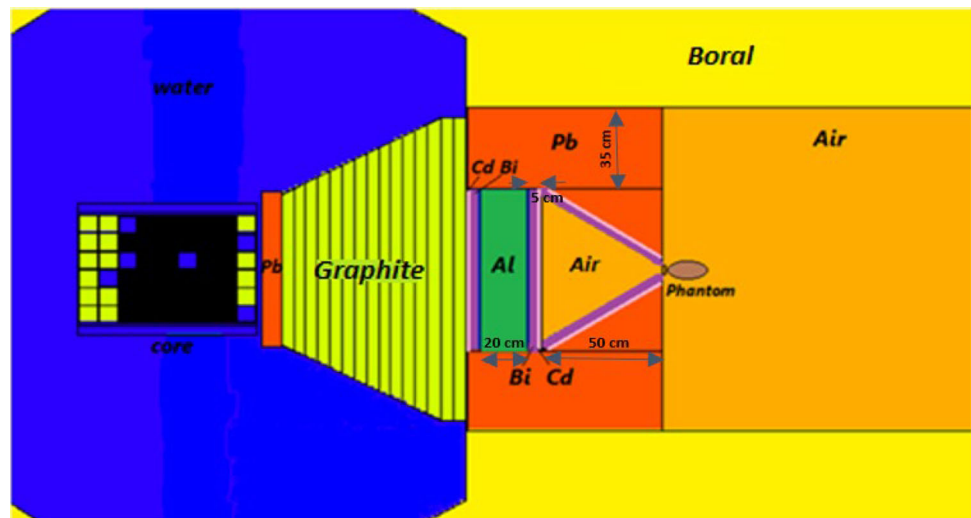
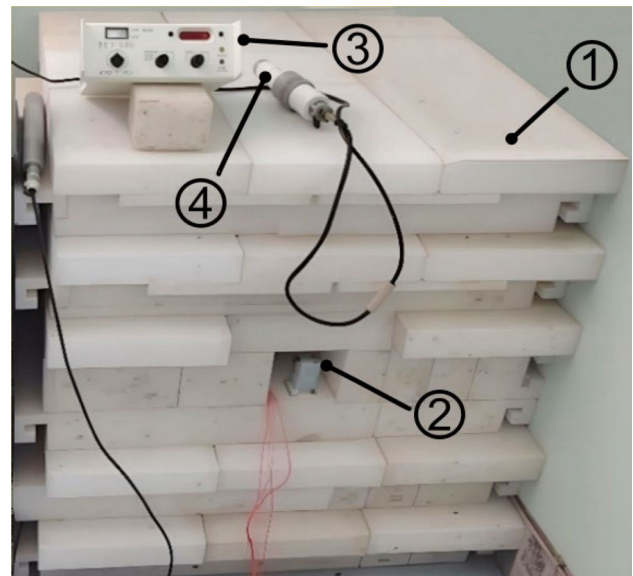


Fig. 5 Prizm-AN experimental installation [27]. Components include: (1) polyethylene prism housing the horizontal measurement channel, (2) IBN-10 type Pu-Be neutron source; (3) MKS-01R scintillator radiometer-dosimeter for radiation monitoring; and (4) helium-3 (^3He) neutron detection unit for thermal neutron measurements



includes cross-section data for 375 isotopes derived from BNAB-93 (1997), LIPAR-5 (2005), ENDF/B-VII.1 (2011), JENDL-4.0 (2011), and JEFF-3.1 (2006), and (2) the supplementary database, MCUDBRF, which incorporates data for an additional 460 isotopes based on the RUSFOND library [33].

2.2 TRR epithermal beam

The Tehran Research Reactor (TRR) is a 5 MW_{th} pool-type research reactor equipped with seven beam tubes of varying sizes and geometries, a medical irradiation room, and a thermal column. To enable the production of a suitable epithermal neutron beam for BNCT, the thermal column can be modified by removing all existing graphite blocks.

As illustrated in Fig. 4, a BSA has been designed and implemented within the thermal column to generate an epithermal neutron beam for BNCT applications [14]. Additionally, it features two 5 cm thick bismuth slabs serving as gamma-ray filters, all encased within a layer of boral for optimal shielding.

2.3 Prizm-AN installation

Prizm-AN (Fig. 5) is an experimental measurement facility comprising a polyethylene prism with a horizontal channel housing a 250 GBq Pu-Be radioisotope neutron source of the internal bounded neutron (IBN) type. The installation is housed within the Neutronic Measurement Laboratory at Tomsk Polytechnic University.

Fig. 6 Computational models of the Prizm-AN installation and the IBN-10 neutron source (all dimensions in cm): **a** cross-sectional view in the y–z plane showing internal geometry and component placement; **b** three-dimensional representation of the full Prizm-AN configuration

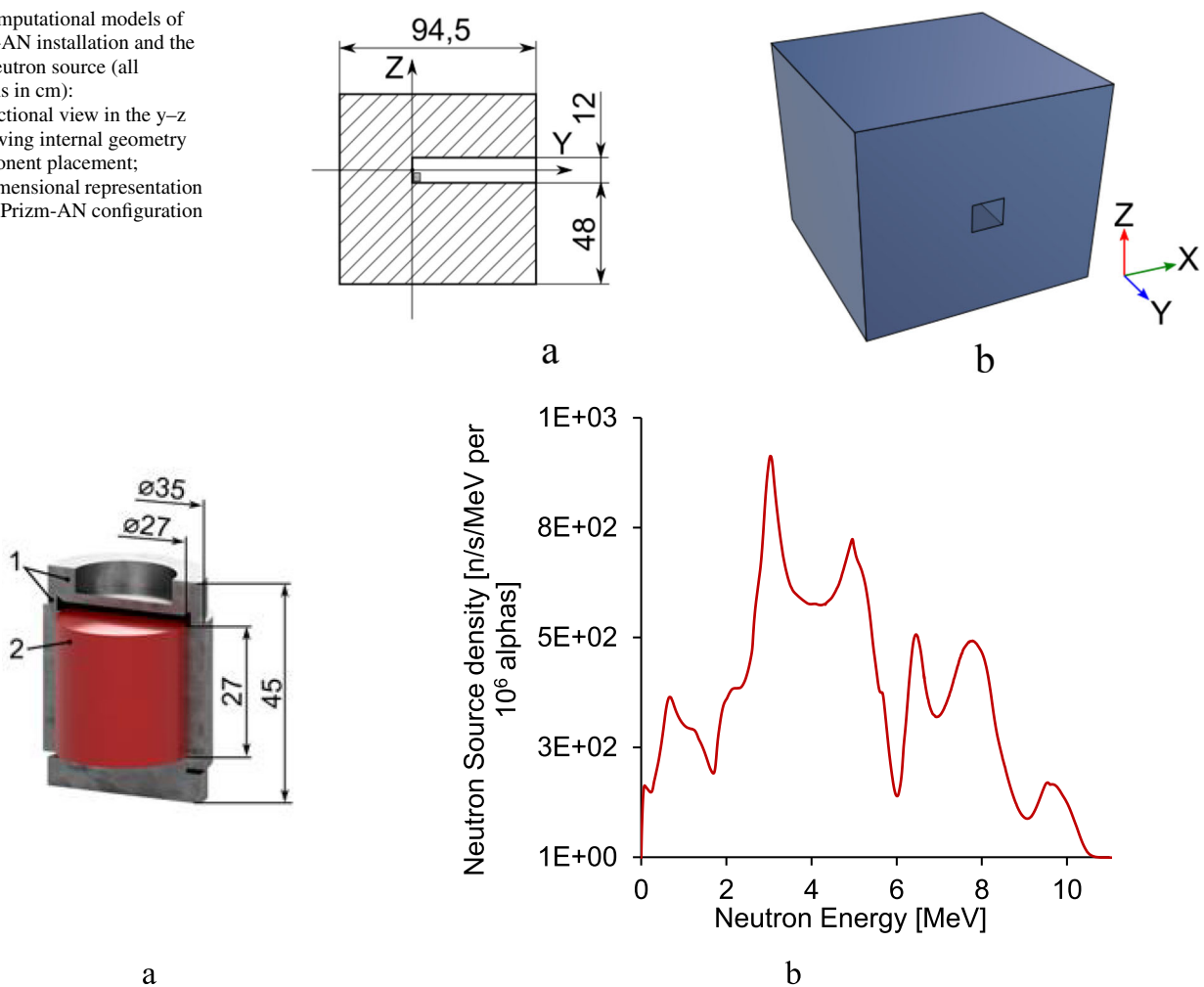


Fig. 7 IBN-10 capsule neutron source: **a** schematic cross-section with dimensions in millimeters, showing (1) the stainless-steel capsule shell and (2) the active region containing the neutron-emitting material; **b** neutron emission spectrum of the IBN-10 radioisotope source

Currently, this laboratory, equipped with Prizm-AN, is actively used for both applied research and academic training in nuclear and neutron physics. Its applications include neutron activation analysis, studies of neutron transport phenomena, and experimental validation of theoretical models.

2.3.1 Calculation models of Prizm-AN and IBN-10

The Prizm-AN measurement installation consists of three primary components [27]: (1) a non-boronated polyethylene prism with an integrated horizontal channel, (2) an IBN-10 capsule-type radioisotope fast neutron source, manufactured by Isotope (<http://www.isotop.ru/>); and (3) a scintillator radiometer-dosimeter, commonly known in Russia as the MKS-01R.

The computational models of the Prizm-AN system and the IBN-10 neutron source are shown in Figs. 6–8a. The polyethylene prism, composed of C_2H_4 with a density of 0.945 g/cm^3 , has a nuclide density of $1.198 \times 10^{-1} \text{ nuclide/(b}\cdot\text{cm)}$. Geometrically, it is designed as a rectangular parallelepiped with dimensions of 90 cm (height) \times 89 cm (width) \times 94.5 cm (depth).

A horizontal rectangular channel is located 48 cm from the base of the prism. This channel measures 13 cm in width, 12 cm in height, and 59.5 cm in depth. It is filled with air, modeled as a gas mixture with an atomic density of $4.99 \times 10^{-5} \text{ nuclide/(b}\cdot\text{cm)}$.

The IBN-10 capsule neutron source, illustrated in Fig. 7, features a cylindrical geometry with a diameter of 3.50 cm and a height of 4.50 cm. The center of the capsule is located at coordinates $x = 44.55 \text{ cm}$, $y = 57.75 \text{ cm}$, and $z = 50.25 \text{ cm}$. The active region of the source, shown in red in Fig. 7a, has a diameter and height of 2.70 cm and is composed of a densely sintered mixture of weapons-grade PuO_2 and beryllium powder.

General technical specifications for the IBN-10 capsule can be found in [27]. The precise material composition of the active region remains proprietary and is not disclosed by the manufacturer. The capsule is double-encapsulated in a stainless-steel shell with an overall density of 7.92 g/cm^3 . The total activity of plutonium isotopes within the source is 250 GBq (approximately 6.8 Ci).

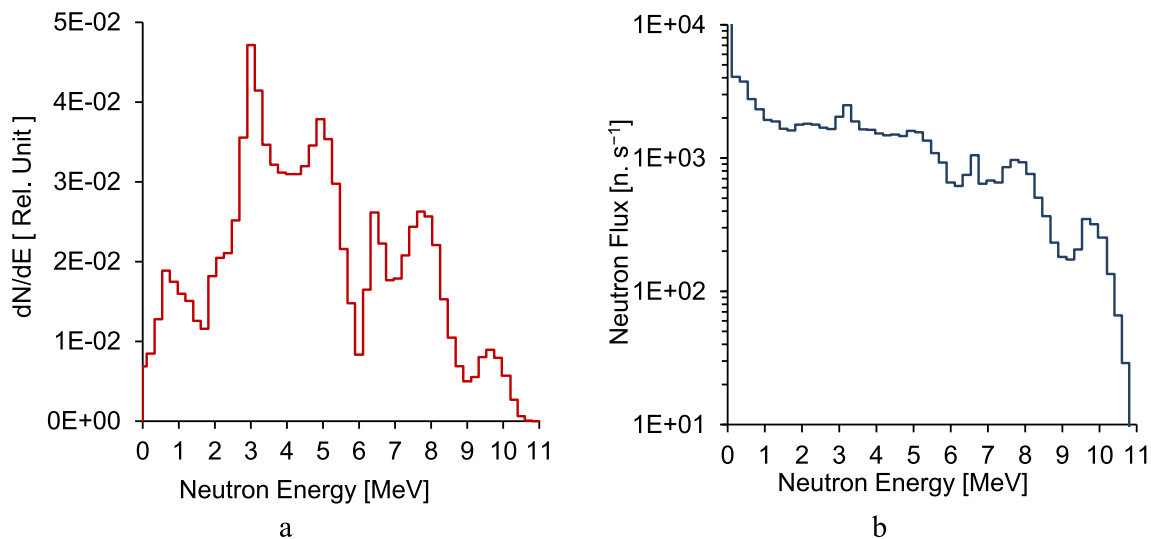


Fig. 8 Neutron spectra of the IBN-10 source: **a** group-wise neutron spectrum; **b** neutron energy spectrum measured within the Prizm-AN channel

According to the manufacturer, the IBN-10 source emits approximately 1.0×10^7 neutrons per second isotropically over 4π steradians. This emission rate has been experimentally verified and is referred to as the measured fast neutron strength (I_n^{exp}).

The unmoderated α -n neutron emission spectrum of the IBN-10 source, normalized to 10^6 α -particles, was calculated using the NEDIS-3 code (for code applications, [34–37]) and is shown in Fig. 7b. The corresponding group spectrum, presented in Fig. 8a ($\int dN/dE = 1$, red curve), was used to reconstruct the total emission yield. The reconstructed neutron yield ($Y_n = 9.03 \times 10^6 \text{ n}\cdot\text{s}^{-1}$) was scaled to match the experimental value I_n^{exp} , ensuring consistency between the measured and simulated fast neutron source strengths.

Using the NEDIS-3 code, we calculated the effective dose rate based on the point-to-point neutron emission spectrum (red curve in Fig. 8a). The calculation employed fluence-to-dose conversion coefficients for anteroposterior exposure geometry as specified in ICRP Publication 116 [38]. The resulting fluence-to-dose conversion factor was determined to be $DF = 1.58 \mu\text{Sv}\cdot\text{h}^{-1}/(\text{n}\cdot\text{cm}^{-2})$. This coefficient serves as a practical conversion factor for rapid estimation of dose rates at specific spatial locations, assuming a uniform neutron field.

In this calculation, the source geometry and any spectral modifications due to scattering or attenuation were neglected. To benchmark our results against previous studies [39, 40], we also computed the ambient dose equivalent rate, $\dot{H}^*(10)$, using ambient dose conversion coefficients expressed in $[\mu\text{Sv}\cdot\text{cm}^2]$ as defined by ICRP Publication 74 [41]. At a distance of 1 m from the IBN-10 source, the ambient dose equivalent rate was calculated to be $141.6 \mu\text{Sv}\cdot\text{h}^{-1}$, which agrees within a relative error margin of $\leq 15\%$ with the data reported by Peleshko et al. [39].

2.3.2 Reference markers for TENIS verification

The emission spectrum data presented in Fig. 8a, obtained in Sect. 2.3.1 and validated through comparison with the reference field reported by Peleshko et al. [39], were used as input for calculating neutron beam parameters within the collimator channel of the Prizm-AN installation and at the channel outlet.

These calculations were performed using the PHITS (Particle and Heavy Ion Transport Code System, Version 2.23) software [42]. The computational models employed are illustrated in Figs. 6, 7, and 8a. A comparison between the PHITS simulation results and corresponding experimental measurements [27] is shown in Fig. 9a. The comparison demonstrates good agreement between the calculated and experimental neutron fluence rates along the entire length of the collimator channel (Fig. 9a, green line, for neutrons with energies $\varphi_{<0.5 \text{ eV}}$), with a maximum uncertainty not exceeding 20%.

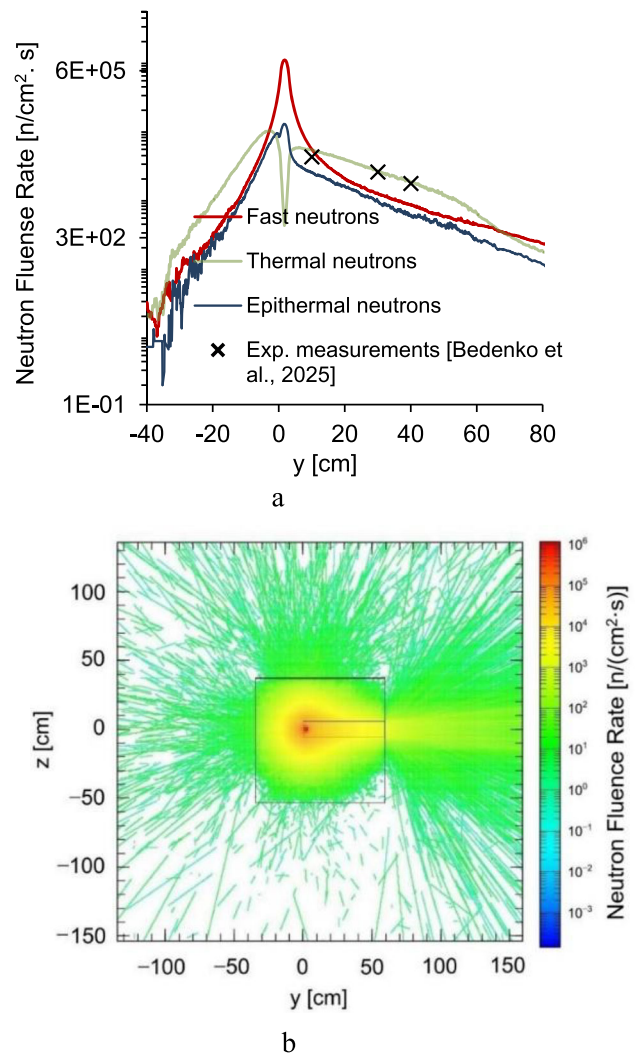
These findings support the use of the datasets shown in Figs. 8b and 9 as reference benchmarks for validating the performance of spectral unfolding algorithms based on ANNs in future TENIS test campaigns.

Due to limited access to the IRT-T and TTR reactors, verification experiments were carried out on the Prizm-AN installation.

2.4 Unfolding the neutron spectrum with TENIS and ANN: max–min problem

The TENIS system comprises seventeen rectangular NE102 plastic scintillators arranged orthogonally: seven horizontal detectors measuring $2 \times 2 \times 20 \text{ cm}^3$ and ten vertical detectors measuring $2 \times 2 \times 14 \text{ cm}^3$. These scintillator arrays are positioned on opposite sides of a rectangular water phantom, segmenting it into seventy voxels of $2 \times 2 \times 15 \text{ cm}^3$ each [19]. TENIS generates a thermal neutron map by detecting 2.22 MeV gamma rays produced via the $^1\text{H}(n_{\text{th}}, \gamma)^2\text{D}$ reaction.

Fig. 9 Spatial and energy distribution of the neutron field along the y-axis: **a** Neutron fluence rate categorized by energy ranges, thermal (10^{-10} to 5×10^{-7} MeV), epithermal (5×10^{-7} to 0.1 MeV), and fast neutrons (0.1–20 MeV); **b** Two-dimensional spatial distribution of neutron fluence rate in the y–z plane



Previous work [16] demonstrated that thermal neutron images reconstructed by TENIS can serve as reliable input for precise unfolding of neutron energy spectra from both monoenergetic and polyenergetic sources. Building on this methodology, the present study aims to determine the energy spectrum of neutrons exiting the BSAs, which predominantly fall within the epithermal energy range. It is important to highlight that real-time neutron spectroscopy in the low-energy regime remains challenging and is associated with considerable uncertainties [23].

Note should be taken that the neutron unfolding is an ill-posed inverse problem in which the number of unknown spectral bins typically exceeds the number of independent measurements [43]. The forward model is $b \approx Ax$, where b is the vector of measured counts in detector channels, x is the true neutron spectrum discretized into energy bins, and A is the detector response matrix that encodes efficiency, resolution, and scattering. Because A is often ill-conditioned and the data are noisy, there exists an infinite family of spectra x that reproduce the measurements within uncertainties; only a subset corresponds to physically plausible spectra. Consequently, without additional information the solution is non-unique and highly sensitive to measurement noise [44]. Most unfolding algorithms rely on regularization or prior information to stabilize the solution and to enforce physical constraints (*e.g.*, nonnegativity, smoothness, or physics-based priors). In practice, many traditional unfolding codes require an initial guess spectrum or prior, to guide the solution toward plausible regions of the solution space. Monte Carlo-based approaches and data-driven artificial intelligence methods offer alternative strategies that can reduce reliance on explicit regularization, but they still depend on a forward model, priors, or training data.

In this study, to unfold the energy spectrum of unknown neutron sources, we constructed the TENIS response matrix using 70-pixel data derived from reconstructed images. This data was obtained by exposing TENIS to 109 monoenergetic neutron beams spanning energies from 10^{-11} MeV to 14.92 MeV, distributed at equi-lethargy intervals. The creation and training of the ANN utilized a driver script developed in MATLAB [16]. Additionally, TENIS was exposed to the BNCT beamlines of the TRR and IRT-T research reactors to acquire 70-pixel thermal neutron images, which were subsequently used for neutron spectroscopy via ANN unfolding.

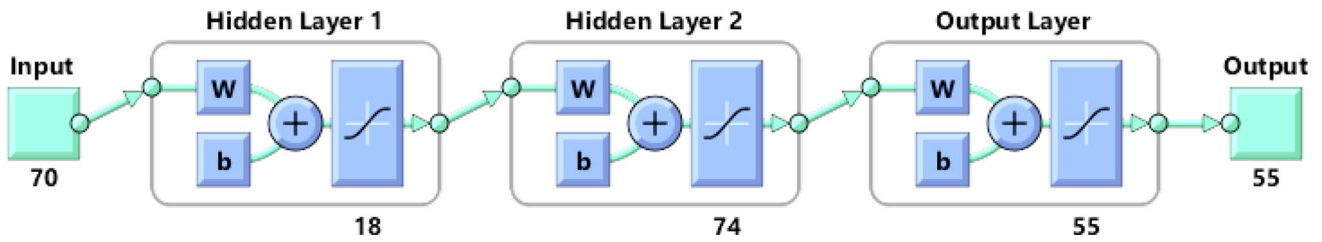


Fig. 10 Architecture of the ANN employed for unfolding the BNCT neutron energy spectrum

The neural network architecture employed for spectrum unfolding consists of three layers: two hidden layers and one output layer, as illustrated in Fig. 10. The Levenberg–Marquardt backpropagation algorithm was used for training, implemented through the MATLAB ANN Toolbox [45]. The *tansig* activation function was applied to neurons in both the hidden and output layers.

To evaluate the agreement between the actual and ANN-unfolded spectra across m energy intervals, we employed the root-mean-square error (RMSE) and the coefficient of determination (R^2) as quantitative metrics. The RMSE and R^2 values were calculated using the following equations [16, 46]:

$$RMSE = \sqrt{\frac{1}{m} \sum_{j=1}^m \left(\phi_E(E)_j^{ANN} - \phi_E(E)_j^{Actual} \right)^2} \quad (1)$$

$$R^2 = 1 - \frac{\sum_{j=1}^m \left(\phi_E(E)_j^{ANN} - \phi_E(E)_j^{Actual} \right)^2}{\sum_{j=1}^m \left(\text{average of } \phi_E(E)_j^{ANN} - \phi_E(E)_j^{Actual} \right)^2} \quad (2)$$

The optimal ANN structure was determined by selecting the configuration that yielded the lowest root-mean-square error (RMSE) and the highest correlation coefficient.

2.5 Minimum detectable activity assessment for TENIS

To accurately determine the smallest signal that can be reliably detected and to establish a detection threshold for the counting system, it is essential to measure the minimum detectable activity (MDA). One of the most widely accepted definitions of MDA was first introduced by Currie [47]. In this framework, N_T represents the total counts recorded from an unknown sample, while N_B denotes the counts recorded from a blank sample, which characterizes the background level. The net counts attributable to the unknown sample are then calculated as follows [48, 49],

$$N_S = N_T - N_B \quad (3)$$

where N_D represents the minimum net counts required to satisfy the detection criterion. This value, N_D , serves as a numerical estimate of the mean net counts corresponding to the MDA and can be derived from Currie's equation [47]:

$$N_D = 4.653\sqrt{N_B} + 2.706 \quad (4)$$

N_D can be now interpreted as the minimum number of radiations needed from the source to achieve sufficient counts. To convert N_D (in counts) to MDA (α), the additional factors of radiation yield per disintegration (f) and absolute detection efficiency (ϵ) must be taken into account where T is the counting time per sample [49]:

$$\alpha = N_D / f\epsilon T \quad (5)$$

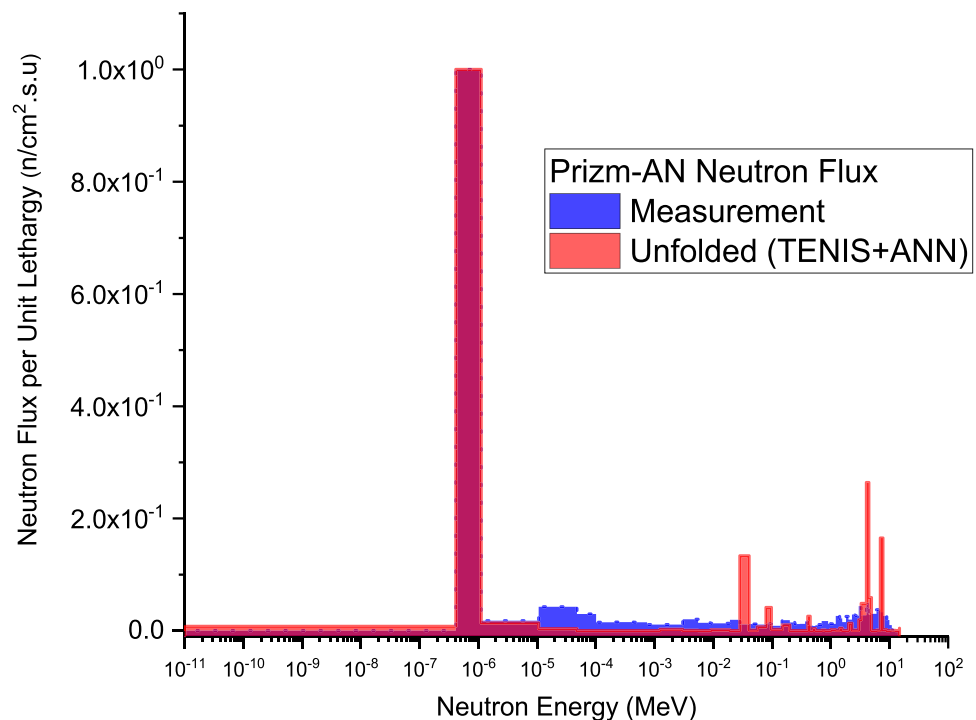
Following the above methodology, the MDA for TENIS, taking into account all seventeen plastic scintillators, was calculated.

2.6 Unfolding the neutron flux of Prism-AN for TENIS system verification

The image data acquired from the TENIS system when exposed to neutron beams from the Prism-AN setup is presented in Fig. 11. This dataset was used as input for the ANN implemented in MATLAB, as described in Sect. 2.4. Figure 11 also displays a comparison between the ANN-unfolded results and the corresponding computational measurements (refer to Sect. 2.3 and Fig. 8b).

The performance of the ANN in unfolding the neutron energy spectrum of the Prism-AN beam was assessed using the correlation coefficient (R^2) and root-mean-square error (RMSE) as evaluation metrics. The resulting R^2 value of 0.992 and RMSE of 0.041 demonstrate excellent agreement between the ANN-unfolded spectrum and the reference computational data. These results highlight the reliability of the proposed ANN-based spectrum unfolding approach and confirm the high accuracy and effectiveness of the developed neutron spectrometry system.

Fig. 11 ANN-unfolded neutron spectrum of Prizm-AN versus the measured results



3 Results and discussion

3.1 Unfolding neutron energy spectra

The image data acquired from the TENIS system when exposed to the therapeutic beamlines of the TRR and IRT-T research reactors are shown in Figs. 12 and 13, respectively. The reconstructed thermal neutron images presented in Figs. 12b and 13b were used as input for the ANN implemented in MATLAB. The resulting unfolded neutron energy spectra for the TRR and IRT-T therapeutic beamlines are presented in Figs. 14 and 15, respectively.

The performance of the ANN in unfolding the neutron energy spectra from the TRR and IRT-T research reactors was evaluated using the correlation coefficient (R^2) and root-mean-square error (RMSE) as quantitative metrics. The correlation coefficients of 0.86 for TRR and 0.74 for IRT-T, along with corresponding RMSE values of 0.014 and 0.020, respectively, demonstrate good agreement between the ANN-unfolded spectra and the reference measurements. These results, particularly the relatively high R^2 values and low RMSEs, further confirm the effectiveness of the proposed spectroscopy system and ANN-based unfolding method for neutron energy spectrum characterization in BNCT applications.

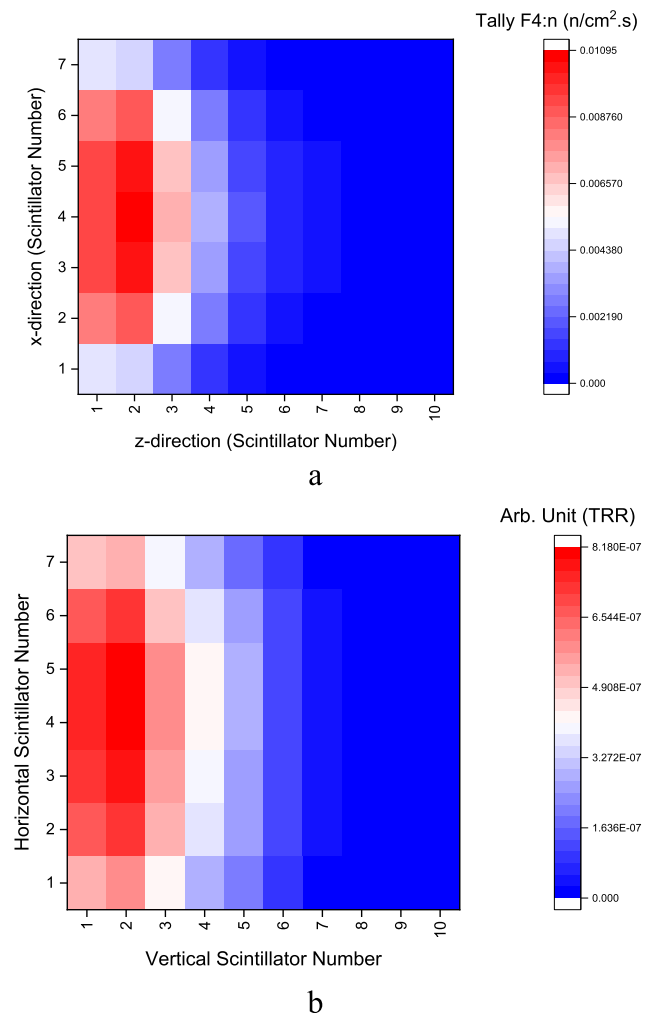
3.2 Measured MDA for TENIS using BNCT spectrum of IRT-T

The influence of background photons on the TENIS system was evaluated using a systematic approach. The gamma-ray spectrum emitted by the IRT-T reactor was used to represent the background radiation, and the corresponding N_D values were calculated for all seventeen detectors. The detector with the highest N_D value was taken as representative of the system-wide minimum detectable net count. Among the seventeen NE102 plastic scintillation detectors, the maximum simulated background count rate was 232 counts per second.

To assess detection capability, the incident neutron flux from the IRT-T reactor was assumed to be 2×10^9 n/cm².s. Under this flux, each detector was required to record counts at least ten times higher than the minimum detection threshold determined by the Currie equation. As a result, it was found that a neutron flux as low as 2×10^8 n/cm².s can still produce sufficient gamma-ray signals to exceed the minimum acceptable count rate.

For the BNCT neutron spectrum at IRT-T, the MDA of the TENIS system was calculated using Eq. (5). This evaluation is critical for determining the absolute detection efficiency (ϵ) of the NE102 plastic scintillators integrated within the TENIS framework. The results confirm that the TENIS detectors are fully capable of reliably detecting 2.22 MeV gamma-rays. This conclusion is supported by the significantly higher count rates observed in the presence of the reactor neutron spectrum compared to those recorded under background-only conditions.

Fig. 12 The 2D thermal neutron map of TENIS when it is exposed to TRR epithermal beam, **a** actual flux values, and **b** reconstructed image



4 Conclusions

In this study, MATLAB software was used to train an ANN for unfolding neutron energy spectra, with a primary focus on the epithermal energy region. The input data for the ANN consisted of reconstructed thermal neutron flux images produced using the MCNP6.1 code in conjunction with the TENIS system. The results demonstrated that neutron spectroscopy using TENIS was highly effective in the epithermal range, enabling accurate and potentially real-time applications in BNCT.

Based on the previous research and current findings, the results support the feasibility of employing TENIS as a neutron spectrometer across the full neutron energy spectrum. However, the system's response to high-intensity neutron beams, particularly the potential for detector saturation, represents a critical aspect that warrants further investigation in future work.

Furthermore, the TENIS system offers a promising platform for exploring the therapeutic efficacy of boron-based compounds, potentially contributing to the optimization of BNCT treatment protocols. Based on the findings of this study, TENIS shows strong potential for the development of advanced neutron detection systems for BNCT and related applications.

Note should be taken that, while ANNs are powerful tools for neutron spectrum unfolding in this study, it is important to acknowledge several limitations, both within this work and in other energy spectrum unfolding applications, including:

Dependence on data quality and representativeness: Effective training requires extensive, high-quality datasets that encompass the full range of neutron spectra. Biased or limited data can impair generalization and result in unreliable outcomes.

Overfitting risks: Without proper regularization, ANNs may overfit training data, capturing noise rather than physical relationships, leading to inaccurate predictions on unseen data.

Limited physical interpretability: Unlike traditional methods based on physical models, ANNs function as so-called black boxes, making it challenging to interpret the unfolding process or validate results physically.

Sensitivity to noise and measurement uncertainty: Input data containing noise or uncertainties can adversely affect ANN outputs, potentially amplifying errors and reducing stability.

Fig. 13 The 2D thermal neutron map of TENIS when it is exposed to IRT-T epithermal beam, **a** actual flux values, and **b** reconstructed image

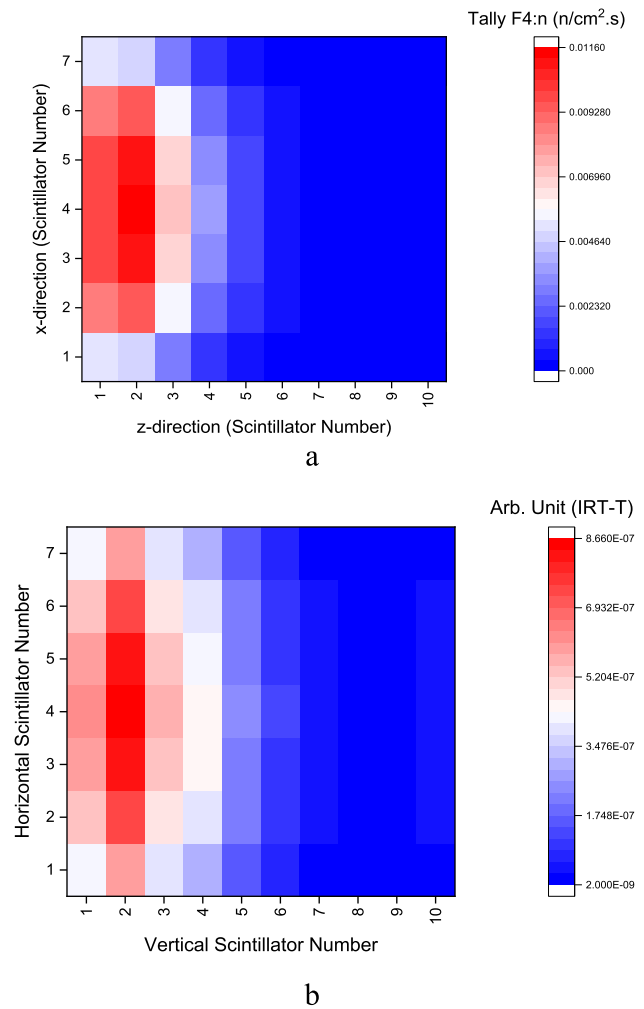
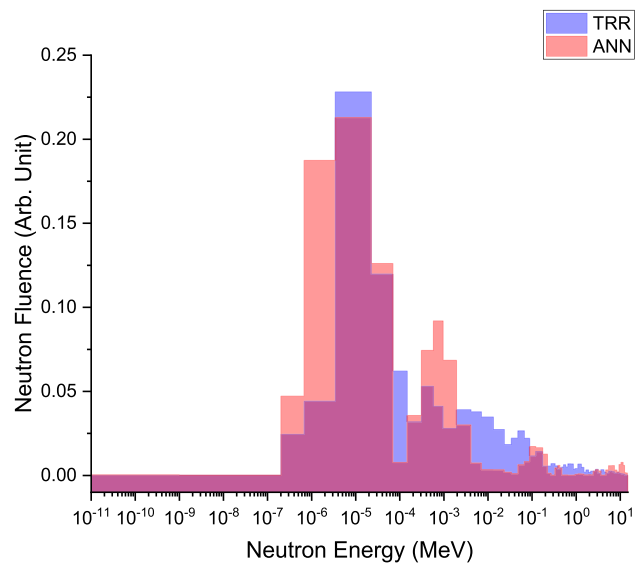


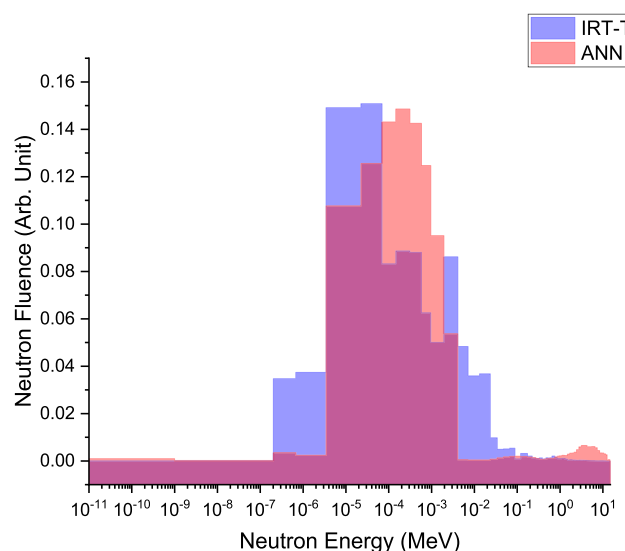
Fig. 14 Unfolded neutron energy spectrum of BNCT beam line in TRR



Computational demands: Training effective ANNs, especially large architectures, can require substantial computational resources and time, including extensive hyperparameter tuning.

Uncertainty quantification challenges: Unlike conventional methods that provide explicit uncertainty estimates, ANNs often lack inherent mechanisms for quantifying confidence in their predictions, complicating result validation.

Fig. 15 Unfolded neutron spectrum of BNCT beam line in IRT-T



Acknowledgements This work was supported by Grant No. 3/55605 (28/06/1400) from the Vice President for Research and Technology of Ferdowsi University of Mashhad. Part of the research was conducted using the core facilities of the «Physical and Chemical Methods of Analysis» center at Toms Polytechnic University (TPU).

Data availability This manuscript has associated data in a data repository. [Authors' comment: The data supporting the findings of this study are available upon request.]

References

1. P.R. Menéndez, B.M.C. Roth, M.D. Pereira, M.R. Casal, S.J. González, D.B. Feld, G.A. Santa Cruz, J. Kessler, J. Longhino, H. Blaumann, R.J. Rebagliati, BNCT for skin melanoma in extremities: updated Argentine clinical results. *Appl. Radiat. Isot.* **67**(7–8), S50–S53 (2009)
2. Y. Nakagawa, T. Kageji, Y. Mizobuchi, H. Kumada, Y. Nakagawa, Clinical results of BNCT for malignant brain tumors in children. *Appl. Radiat. Isot.* **67**(7–8), S27–S30 (2009)
3. R.F. Barth, J.C. Grecula, Boron neutron capture therapy at the crossroads—where do we go from here? *Appl. Radiat. Isot.* **160**, 109029 (2020)
4. R.F. Barth, G. Wu, M.D.G.H. Vicente, J.C. Grecula, N. Gupta, Boron neutron capture therapy of cancer: where do we stand now? *Cancer Commun.* **44**(8), 889–892 (2024)
5. T.E. Blue, J.C. Yanch, Accelerator-based epithermal neutron sources for boron neutron capture therapy of brain tumors. *J. Neurooncol.* **62**, 19–31 (2003)
6. M.A. Dymova, S.Y. Taskaev, V.A. Richter, E.V. Kuligina, Boron neutron capture therapy: current status and future perspectives. *Cancer Commun.* **40**(9), 406–421 (2020)
7. M. Suzuki, Boron neutron capture therapy (BNCT): a unique role in radiotherapy with a view to entering the accelerator-based BNCT era. *Int. J. Clin. Oncol.* **25**, 43–50 (2020)
8. H. Zhang, R. Wang, Y. Yu, J. Liu, T. Luo, F. Fan, Glioblastoma treatment modalities besides surgery. *J. Cancer* **10**(20), 4793–4806 (2019)
9. S. Lillo, A. Mirandola, A. Vai, A.M. Camarda, S. Ronchi, M. Bonora, R. Ingargiola, B. Vischioni, E. Orlandi, Current status and future directions of proton therapy for head and neck carcinoma. *Cancers* **16**(11), 2085 (2024)
10. S. Bagherzadeh-Atashchi, N. Ghal-Eh, F. Rahmani, R. Izadi-Najafabadi, S.V. Bedenko, Design of beam line for BNCT applications in HEC-1 channel of IRT-T research reactor. *Radiat. Phys. Chem.* **215**, 111368 (2024)
11. Y.B. Chertkov, M.N. Anikin, I.I. Lebedev, A.G. Naimushin, N.V. Smol'nikov, Calculation and experimental determination of the neutronics characteristics of the IRT-T research reactor. *At. Energ.* **131**(1), 42–45 (2021)
12. M.V. Shchurovskaya, V.P. Alferov, N.I. Geraskin, A.I. Radaev, A.G. Naymushin, Y.B. Chertkov, M.N. Anikin, I.I. Lebedev, Control rod calibration simulation using Monte Carlo code for the IRT-type research reactor. *Ann. Nucl. Energy* **96**, 332–343 (2016)
13. E. Bavarnegin, A. Sadremontaz, H. Khalafi, Y. Kasesaz, M. Golshanian, H. Ghods, A. Ezzati, M. Keyvani, M. Haddadi, Measurement and simulation of the TRR BNCT beam parameters. *Nucl. Instrum. Methods Phys. Res. Sect. A Accel. Spectrom. Detect. Assoc. Equip.* **830**, 53–58 (2016)
14. Y. Kasesaz, H. Khalafi, F. Rahmani, Design of an epithermal neutron beam for BNCT in thermal column of Tehran research reactor. *Ann. Nucl. Energy* **68**, 234–238 (2014)
15. M.M. Vanani, Y. Kasesaz, M. Hosseinpanah, A. Akhound, Collimated neutron beam design for TRR thermal column. *J. Instrum.* **16**(12), P12023 (2021)
16. S. Bagherzadeh-Atashchi, N. Ghal-Eh, F. Rahmani, R. Izadi-Najafabadi, S.V. Bedenko, Neutron spectroscopy with TENIS using an artificial neural network. *Appl. Radiat. Isot.* **201**, 111035 (2023)
17. R. Bedogni, J.M. Gómez-Ros, A. Pola, M. Treccani, M. Costa, CYSP-HS: a new version of the CYSP directional neutron spectrometer with increased sensitivity. *Appl. Radiat. Isot.* **142**, 38–41 (2018)
18. R. Bedogni, M.A. Caballero-Pacheco, L. Russo et al., Rad-hard silicon carbide thermal neutron detectors for quality assurance in BNCT. *Eur. Phys. J. Plus* **140**(247), 1 (2025)
19. N. Ghal-Eh, S. Green, A plastic scintillator-based 2D thermal neutron mapping system for use in BNCT studies. *Appl. Radiat. Isot.* **112**, 31–37 (2016)
20. Z. Kazemi, F. Rahmani, N. Ghal-Eh, V. Bedenko, Optimization of a multi-moderator neutron spectrometer for use in epithermal neutron spectrum measurements in BNCT. *Eur. Phys. J. Plus* **140**(5), 1–8 (2025)
21. B. Liu, H. Lv, H. Xu, L. Li, W. Li, F. Jing, Y. Wu, Study on neutron spectrum unfolding method of organic scintillation measurement based on iterative regularization. *Ann. Nucl. Energy* **162**, 108504 (2021)

22. J. Prateepkaew, N. Matsubayashi, T. Takata, H. Tanaka, Y. Sakurai, Characteristic comparison between two different neutron spectrometers for boron neutron capture therapy irradiation field developed at heavy-water neutron irradiation facility of Kyoto University research reactor. *Appl. Radiat. Isot.* (2025). <https://doi.org/10.1016/j.apradiso.2025.111717>
23. F. Rahmani, N. Ghal-Eh, H.R. Vega-Carrillo, A multi-moderator neutron spectrometer for use in BNCT studies of the Tehran research reactor. *Appl. Radiat. Isot.* **174**, 109751 (2021)
24. H. Vega-Carrillo, A. Baltazar-Raigosa, V.M. Hernández-Dávila, E. Gallego, G.F. García-Fernández, S.V. Bedenko, Monte carlo design of a novel passive regular parallelepiped neutron spectrometer (TLD600/RPS). *Radiat. Phys. Chem.* **236**(1), 112861 (2025)
25. G.Y. Wang, R. Han, J.L. Liu, X.P. Ouyang, J.C. He, J.Y. Yan, Comparison and research on the GRAVEL and PRIP algorithms of neutron energy spectrum unfolding. *Radiat. Detect. Technol. Methods* **1**(2), 1–6 (2017)
26. H. Yazdandoust, N. Ghal-Eh, M.M. Firoozabadi, TENIS—Thermal neutron imaging system for use in BNCT. *Appl. Radiat. Isot.* **176**, 109755 (2021)
27. S.V. Bedenko, G.N. Vlaskin, S.D. Polozkov, N. Ghal-Eh, A.S. Demin, D.G. Veretennikov, H.R. Vega-Carrillo, Parameters of the neutron field at the Prizm-AN stand in the neutronic measurement laboratory. *Appl. Radiat. Isot.* **219**, 111729 (2025)
28. V. Conte, A. Bianchi, A. Selva, Boron neutron capture therapy: microdosimetry at different boron concentrations. *Appl. Sci.* **14**(1), 216 (2023)
29. X. Zhang, Y. Lin, Developments in neutron sources for boron neutron capture therapy. In *Frontiers in Boron-based Medicinal Chemistry*, 115–216 (2023)
30. S.V. Bedenko, I.O. Lutsik, V.V. Prihodko, A.A. Matyushin, S.D. Polozkov, V.M. Shmakov, H.R. Vega-Carrillo, Fusion-fission hybrid reactor with a plasma source of deuterium-tritium neutrons in a linear configuration. *Prog. Nucl. Energy* **154**, 104477 (2022)
31. S.V. Bedenko, S.D. Polozkov, A.S. Demin, N. Ghal-Eh, F. Rahmani, H.R. Vega-Carrillo, Neutron pumping of active medium formed by gadolinium isotopes ^{155}Gd and ^{156}Gd pair: a feasibility study. *Appl. Radiat. Isot.* **206**, 111232 (2024)
32. M.A. Kalugin, D.S. Oleynik, D.A. Shkarovsky, Overview of the MCU Monte Carlo software package. *Ann. Nucl. Energy* **82**, 54–62 (2015)
33. V.N. Koshcheev, G.N. Manturov, M.N. Nikolaev, A.M. Tsibouliya, Verification of neutron data for main reactor materials from RUSFOND library based on integral experiments. In *EPJ Web of Conferences* (Vol. 42, p. 07006). EDP Sciences (2013)
34. S.V. Bedenko, G.N. Vlaskin, N. Ghal-Eh, I.O. Lutsik, R. Irkimbekov, F. Rahmani, H.R. Vega-Carrillo, Nedis-serpent simulation of a neutron source assembly with complex internal heterogeneous structure. *Appl. Radiat. Isot.* **160**, 109066 (2020)
35. F. Rahmani, N. Ghal-Eh, S.V. Bedenko, Landmine-identification system based on the detection of scattered neutrons: a feasibility study. *Radiat. Phys. Chem.* **199**, 110264 (2022)
36. G.N. Vlaskin, S.V. Bedenko, N. Ghal-Eh, H.R. Vega-Carrillo, Neutron yield and energy spectrum of $^{13}\text{C}(\alpha, n)^{16}\text{O}$ reaction in liquid scintillator of KamLAND: a Nedis-2m simulation. *Nucl. Eng. Technol.* **53**(12), 4067–4071 (2021)
37. G.N. Vlaskin, S.V. Bedenko, S.D. Polozkov, N. Ghal-Eh, F. Rahmani, Neutron and gamma-ray signatures for the control of alpha-emitting materials in uranium production: a Nedis2m-MCNP6 simulation. *Radiat. Phys. Chem.* **208**, 110919 (2023)
38. ICRP, Conversion Coefficients for use in Radiological Protection against External Radiation. ICRP Publication 116. *Ann. ICRP* **40** (2–5) (2010)
39. V.N. Peleshko, E.N. Savitskaya, A.V. Sannikov, M.M. Sukharev, A.G. Muzoverov, ^{239}Pu -Be-source based neutron reference fields. *At. Energ.* **126**, 313–319 (2019)
40. H.R. Vega-Carrillo, E. Manzanares-Acuña, A.M. Becerra-Ferreiro, A. Carrillo-Núñez, Neutron and gamma-ray spectra of $^{239}\text{PuBe}$ and $^{241}\text{AmBe}$. *Appl. Radiat. Isot.* **57**(2), 167–170 (2002)
41. ICRP, Conversion Coefficients for use in Radiological Protection against External Radiation. ICRP Publication 74. *Ann. ICRP* **26**(3–4) (1996)
42. K. Niita, N. Matsuda, Y. Iwamoto, T. Sato, H. Nakashima, Y. Sakamoto, H. Iwase, L. Sihver, *PHITS: Particle and heavy ion transport code system*, version 2.23 (2010)
43. M.R. Kardan, S. Setayeshi, R. Koohi-Fayegh, M. Ghiassi-Nejad, Neutron spectra unfolding in Bonner spheres spectrometry using neural networks. *Radiat. Prot. Dosimetry* **104**(1), 27–30 (2003)
44. H.R. Vega-Carrillo, V.M. Hernández-Dávila, E. Manzanares-Acuña, E. Gallego, A. Lorente, M.P. Iniguez, Artificial neural networks technology for neutron spectrometry and dosimetry. *Radiat. Prot. Dosimetry* **126**(1–4), 408–412 (2007)
45. MATLAB, The MathWorks Inc., Natick, USA
46. B.T. Pham, S.K. Singh, H.B. Ly, Using artificial neural network (ANN) for prediction of soil. *Vietnam J. Earth Sci.* **42**(4), 311–319 (2020)
47. L.A. Currie, Limits for qualitative detection and quantitative determination. Application to radiochemistry. *Anal. Chem.* **40**(3), 586–593 (1968)
48. G. Gilmore, *Practical Gamma-Ray Spectroscopy* (John Wiley & Sons, 2008)
49. G.F. Knoll, *Radiation Detection and Measurement*. Fourth Edition. John Wiley & Sons (2010)

Springer Nature or its licensor (e.g. a society or other partner) holds exclusive rights to this article under a publishing agreement with the author(s) or other rightsholder(s); author self-archiving of the accepted manuscript version of this article is solely governed by the terms of such publishing agreement and applicable law.